Emergent nonlinear phenomena in discrete-time quantum walks

J. P. Mendonça ⬡,[*] F. A. B. F. de Moura ⬡, M. L. Lyra ⬡, and G. M. A. Almeida

Instituto de Física, Universidade Federal de Alagoas, 57072-900 Maceió, AL, Brazil

Quantum walks are important tools for the development of quantum algorithms and carrying out quantum simulations. Recent interest in nonlinear discrete-time quantum walks aims to use it as a shortcut through dynamical regimes hard to obtain using current methods. We introduce a model featuring a modified conditional shift operator to carry dependence on the local occupation probability with a given strength we are able to control. It accounts for a third-order nonlinear contribution which is found in many physical contexts. We find a rich set of dynamical profiles, including solitonlike propagation, self-trapping, and chaos, all these arising from rather simple rules. Our tool set goes beyond unitary transformations, thus broadening the possibilities for controlling quantum dynamics.

I. INTRODUCTION

Quantum walks are a valuable tool set in the field of quantum information processing [1–3]. More than being just the quantum-mechanical counterpart of the well-known random walk problem, they can be applied for quantum simulation of, e.g., quantum phase transitions [4,5], topological phases [6–8], and even high-energy physics [9], as well as for designing quantum algorithms [10,11]. Moreover, it was shown that both the continuous- and discrete-time versions of the quantum walk allow for universal quantum computation [12,13]. There is even more to it, as equivalencies between quantum walks and relativistic quantum mechanics have been pointed out under proper continuum limits [14–16].

In the discrete-time quantum walk (DTQW) framework [1], the walker is augmented with a set of internal states whereupon a so-called coin operator is defined in order to shuffle (that is, to generate superpositions) them. Following this, a second ingredient, namely, the conditional shift operator, is needed to spread them out in space, wherein transitions from one site to another depend on the internal (coin) state of the walker. This two-step procedure is then repeated as many times as it takes to obtain the desired effect. Experimental realizations of DTQWs have been reported on superconducting systems [6], NMR [17], ion traps [18], ultracold atoms in optical lattices [19], and photonic devices [7,8,20], to name a few.

In essence, quantum walks can be viewed as a kind quantum cellular automata [14,21–24], where one assigns a bunch of complex-valued probability amplitudes and *designs* proper update procedures following the rules of quantum mechanics. Instead of coming up with a Hamiltonian model for a system of interest, the DTQW approach thus offers a different route to explore the Hilbert space. From that point of view, there are endless possibilities for what DTQWs are able to realize, and this is why they are being so largely explored.

A paramount goal is then to reach to ubiquitous dynamical regimes never once attained, if not impossible to, using current methods. A perfect example can be found in a recent work [25], where the authors approached the problem of wave-packet spreading in a nonlinear and disordered medium using a DTQW model and managed to outperform previous computational efforts over about four decades, thereby suggesting that the subdiffusion process occurring due to the interplay between chaotic dynamics and Anderson-localized modes persists asymptotically. Such a remarkable performance of the DTQW is due to its very discrete nature, for a single evolution step has enough information to create shortcuts in the Hilbert space, when comparing to the natural (Hamiltonian-driven) continuous evolution of an equivalent quantum system, possibly demanding longer coherence times or being computationally hard to solve numerically.

The results mentioned above make a strong case for the prospect of using DTQWs to simulate various nonlinear quantum phenomena. Although linearity is inherent to quantum mechanics, emergent nonlinear models are obtained in many situations, such as the Gross-Pitaevskii model which accounts for the dynamics of Bose-Einstein condensates within the mean-field approximation. It was not until recently that fair interest has been given to nonlinear DTQWs [25–33]. In [26], the authors worked out a version of the so-called optical Galton board adapted to include a Kerr-type nonlinearity, implying a self-phase gain in each step of the DTQW procedure, prior to the "coin tossing" operation. They reported on a rich set of dynamical regimes upon varying the nonlinearity parameter, including solitonlike wave-packet propagation and chaotic behavior. Very recently, it has been shown in [33] that certain coin (rotation) angles lead the walker to a self-trapping regime. Another interesting aspect is that the continuous limit of the nonlinear optical Galton board was proved to be a nonlinear Dirac equation [29]. Nonlinear DTQWs with position-dependent coins were explored in [27,28]. Rigorous mathematical treatment of nonlinear DTQWs can be found in [34,35].

_____
*jpedromend@gmail.com

In view of the capability of harnessing quantum cellular automata to reproduce ubiquitous nonlinear properties, in this paper we introduce a DTQW framework where the conditional shift operator is modified to carry a dependence on the local occupation probability attached to given strength α we are able to control. The model accounts for an effective third-order nonlinear contribution which is quite common in nature, such as, for example, in electronic systems [36,37], in the propagation of optical waves in matter [38,39], and in Bose-Einstein condensates [40,41].

By assessing different levels of nonlinearity, we characterize the formation of dispersionless, solitonlike wave packets and also spot a regime featuring self-trapping prior the their appearance. Furthermore, we find that the walker's first moment velocity in the limit $\alpha \approx 0$ approaches $1/\sqrt{2}$, thereby outperforming the linear case. For high enough α, the walker develops chaotic dynamics, meaning that it becomes very sensitive to initial conditions. At last, a sharp transition into a chaotic regime is identified via numerical evaluation of the associated Lyapunov coefficients.

II. NONLINEAR DTQW MODEL

Let $H = H_C \bigotimes H_p$ be the full quantum walk Hilbert space, where H_p comprises the spatial degrees of freedom $\{|n\rangle\}$, with $n \in \mathbb{Z}$, and H_C denotes the two-level coin space, that is $\{|\uparrow\rangle, |\downarrow\rangle\}$. In the usual (linear) procedure, starting from an initial state $|\Psi(t = 0)\rangle$, temporal evolution is performed via the unitary operator $U = S(C \otimes I)$, where S is the conditional shift (translation) operator whose effect is $S|x, \uparrow\rangle = |x + 1, \uparrow\rangle$ and $S|x, \downarrow\rangle = |x - 1, \downarrow\rangle$, C is the coin operator, here taken to be the Hadamard gate $C = (|\uparrow\rangle\langle\uparrow| + |\uparrow\rangle\langle\downarrow| + |\downarrow\rangle\langle\uparrow| - |\downarrow\rangle\langle\downarrow|)/\sqrt{2}$, and I stands for identity operator. After t steps, an arbitrary state reads

$$|\Psi(t)\rangle = \sum_x (m_{x,\uparrow}(t)|x, \uparrow\rangle + m_{x,\downarrow}(t)|x, \downarrow\rangle), \quad (1)$$

with $P_x \equiv |m_{x,\uparrow}|^2 + |m_{x,\downarrow}|^2$ being the probability of finding the walker at the xth site.

We are now to introduce the nonlinear DTQW model, here built upon modifying the conditional shift operator to become dependent on the local occupation probability P_x as

$$S_{nl}|x, \uparrow\rangle = \frac{1}{\sqrt{1 + (\alpha P_x)^2}}(|x + 1, \uparrow\rangle + \alpha P_x|x, \uparrow\rangle), \quad (2)$$

$$S_{nl}|x, \downarrow\rangle = \frac{1}{\sqrt{1 + (\alpha P_x)^2}}(|x - 1, \downarrow\rangle + \alpha P_x|x, \downarrow\rangle), \quad (3)$$

where $\alpha > 0$ accounts for the nonlinearity strength (by setting $\alpha = 0$ the linear version is recovered). The second term on the right-hand side drives the walker into self-trapping at sites featuring high occupation probability. Such a nonlinear mechanism emerges in many contexts [36–41]. In electronic systems it accounts for an underlying coupling with lattice vibrations [36,37]. In optical lattices, it results from high-order susceptibilities due to nonlinear polarization effects [38,39]. Self-trapping is also promoted by interparticle interactions in Bose-Einstein condensates [40,41]. In these systems, the combined action of nonlinear self-trapping and dispersion

leads to solitonlike wave transport, a phenomenon we are about to address in detail for the present nonlinear model.

By inspecting Eqs. (2) and (3), we see that when nonlinearity is weak ($\alpha \approx 0$), the square root approaches 1 and αP_x becomes relevant only if the local probability is large enough. In this case, even though the dynamics is mostly linear, the nonlinear component rapidly builds up given the initial state is fully localized. This entails significant changes in the dispersion profile of the wave function, becoming visibly less dispersive (solitonlike) in the regime of strong nonlinearity ($\alpha \gg 1$).

The evolved state after t steps is obtained via the nonunitary (hence irreversible) evolution $|\Psi(t)\rangle = [S_{nl}(C \otimes I)]^t|\Psi(t = 0)\rangle$ of a symmetric input prepared at the middle of the chain ($x_0 = 0$), $|\Psi(t = 0)\rangle = (|x_0, \uparrow\rangle + i|x_0, \downarrow\rangle)/\sqrt{2}$, with N always set so as to avoid boundary effects. Because the above procedure does not preserve the norm, we reset $|\Psi\rangle \to |\Psi\rangle/\sqrt{\langle\Psi|\Psi\rangle}$ after each step. Nonunitary update rules had been envisaged in the context of quantum cellular automata [21,22] before quantum walks became popular and broaden up the possibilities for tuning quantum dynamics (see [42], for instance). We also mention that nonunitary DTQWs have been increasingly investigated [5,7,8,43–46]. This is usually brought into the framework upon including measurements, gain/loss, and other decoherent processes. Recent experimental progress in photonic platforms has made possible exploration of topological phenomena [5,7,8] and light dynamics through parity-time symmetric lattices [47–50] using nonunitary quantum walks.

As single-particle quantum walks are primarily driven by interference, optical systems relying on coherent light propagation have been a major platform for their implementation, given the easiness of state preparation, port control, and measurement [51]. One particular setting is based on encoding the walker position as pulse arrival times [46–50,52–59]. It basically consists of two fiber loops of different lengths connected via a 50:50 coupler as shown in Fig. 1(a). The pulse propagating through the shorter (longer) loop is then advanced (delayed) in time, which is interpreted as a reduction (increase) of the spatial coordinate by 1 [see Fig. 1(b)]. A crucial advantage of such architecture is that the output is recurrently supplied as input, with some intensity being sent out to fast photodiodes for detection at the end of every round so as to record the walker dynamics. Compared to encoding the walker's position in actual space—say, in a Galton board–like configuration [similar to Fig. 1(b)]—the time-multiplexing scheme saves a great deal of resources (alignment, cost, etc.), thereby allowing for realization of many quantum walk steps [47–49,55,57]. Those are particularly suitable for our nonlinear DTQW model, as the modified shift operator S_{nl} must be fed with the local quantum-mechanical probabilities—light intensities in optics—at every step [see Eqs. (2) and (3)], which demands active readout-feedback procedures. The recursive relations for the light evolution have the form (before normalization)

$$m_{x,\uparrow}(t + 1) = \Gamma_{x-1}(t)[m_{x-1,\uparrow}(t) + m_{x-1,\downarrow}(t)]$$
$$+ \alpha P_x(t)\Gamma_x(t)[m_{x,\uparrow}(t) + m_{x,\downarrow}(t)], \quad (4)$$

$$m_{x,\downarrow}(t + 1) = \Gamma_{x+1}(t)[m_{x+1,\uparrow}(t) - m_{x+1,\downarrow}(t)]$$
$$+ \alpha P_x(t)\Gamma_x(t)[m_{x,\uparrow}(t) - m_{x,\downarrow}(t)], \quad (5)$$
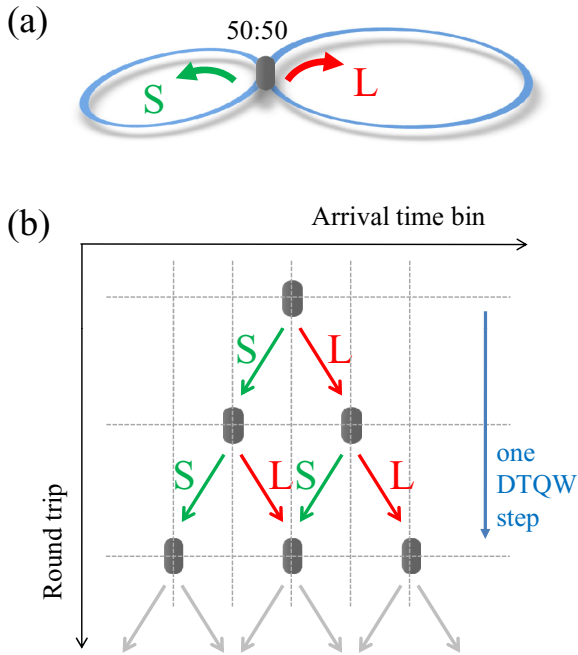
FIG. 1. (a) Two coupled-fiber loops of different lengths are connected by a 50:50 fiber coupler in order to induce a time delay between them. This arrangement is isomorphic to (b) an optical network spanned by pulse arrival times, taking the role of positions vs number of round trips. S (L) stands for short (long) loop, which reduces (advances) the position coordinate by 1. Considering the standard time-multiplexing architecture [47], a single step in our DTQW model must correspond to two consecutive round trips through the coupled-fiber system so as to fulfill Eqs. (4) and (5).

where $\Gamma_x(t) = [1 + (\alpha P_x(t))^2]^{-1/2}$ and $\alpha P_x(t)\Gamma_x(t)$ (both <1 for $\alpha \neq 0$) are loss parameters featuring embedded nonlinearity as they depend on the local intensity $P(x)$. Fine tuning of amplitude modulations can be introduced upon adding acousto-optic modulators in each loop, as seen in Refs. [47–50], for example. Also note that as each local amplitude feeds itself in a single iteration, a DTQW step should correspond to two round trips in the time-multiplexing usual arrangement [47,54], as indicated in Fig. 1(b). The cumulative effect of the above iterative process is such that it yields an increase of the total intensity, which calls for normalization before initiating another step and may be incorporated through another output-based loss, this time at a common rate $1/\sqrt{\langle\Psi|\Psi\rangle}$ for all amplitudes. We finally mention that soliton dynamics has been experimentally probed in 1D [49] and 2D [50] nonlinear DTQWs via synthetic photonic discrete lattices based on time multiplexing by incorporating judiciously controlled gain and loss (nonunitarity).

III. SOLITON DYNAMICS

To begin our analysis, let us take a look at the overall dynamical profile for various values of α as shown in Fig. 2. For the sake of comparison, Fig. 2(a) shows the linear, Hadamard walk, where the wave function is known to go toward a delocalized state asymptotically and its standard deviation
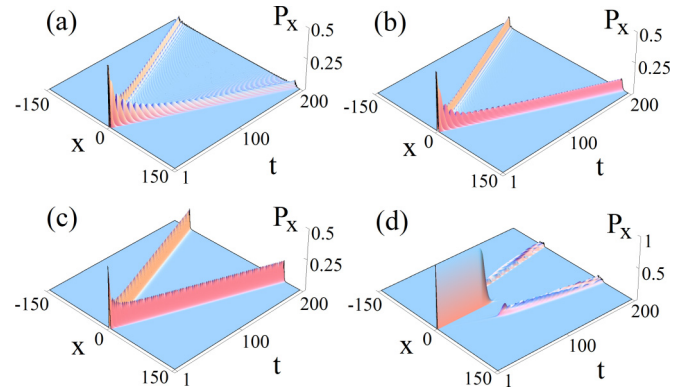

FIG. 2. Time evolution of probability $P_x(t)$ in space for (a) $\alpha = 0$ (linear DTQW), (b) $\alpha = 0.2$, (c) $\alpha = 1$, and (d) $\alpha = 50$. N is set large enough to ensure the wave function does not reach the border and the initial state is the symmetric one, $|\Psi(t = 0)\rangle = (|x_0, \uparrow\rangle + i|x_0, \downarrow\rangle)/\sqrt{2}$ for $x_0 = 0$.

$\sigma \sim t$ entailing a ballistic spreading [2]. In the presence of a low degree of nonlinearity, as seen in Fig. 2(b) for $\alpha = 0.2$, we note the onset of solitonlike behavior, becoming sharper as α is further increased in Figs. 2(c) and 2(d). Another interesting aspect to note from Fig. 2(d) is that those solitonlike structures are formed after a transient time during which the initial state is self-trapped until it suddenly breaks down into a pair of traveling solitonlike pulses departing at a distance from the origin.

We have checked that solitonlike structures emerge for any $\alpha \neq 0$ via the asymptotic behavior of the single-pulse (that is half of the wave function) dispersion $\sigma_{\text{sp}}(t) = \sqrt{\sum_{x=0}^{\infty}(x - \langle x(t)\rangle)^2 P_x(t)}$, with $\langle x(t)\rangle = \sum_{x=0}^{\infty} x P_x(t)$ and $P_x(t)$ being properly normalized in that interval.

Figure 3 shows two distinct dynamical profiles depending on the degree of nonlinearity. To get into that, we shall define
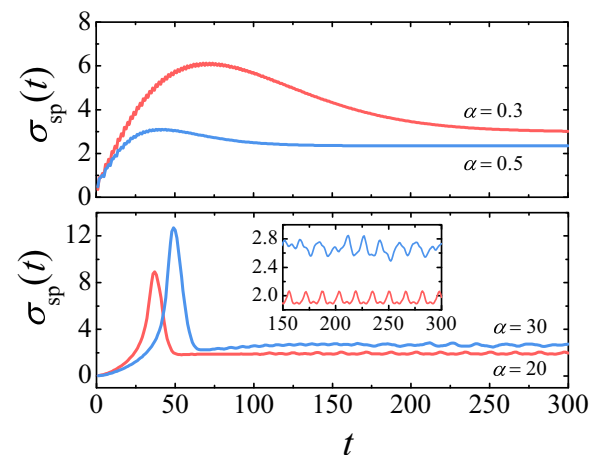

FIG. 3. Single-pulse dispersion $\sigma_{\text{sp}}(t)$ for $\alpha = 0.3, 0.5$ (top panel) and $\alpha = 20, 30$ (bottom panel). The stationary regime of $\sigma_{\text{sp}}(t)$ indicates formation of a stable solitonlike pulse. Here we define the soliton formation time τ as the instant σ_{sp} reaches its maximum. The inset of the bottom panel shows the same curves, zoomed in for better visualization of the stationary regime.
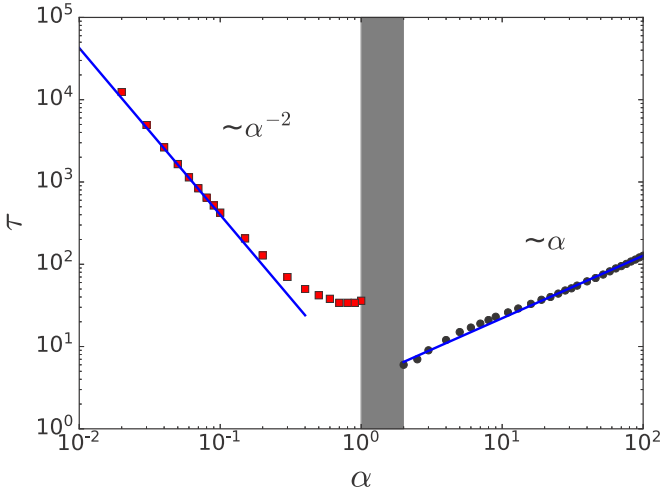
FIG. 4. Soliton formation time τ vs α as evaluated via the single-pulse dispersion dynamics (see text). There are two dynamical regimes, one of which is characterized by $\tau \sim \alpha^{-2}$ (left side) and the other (right side) by $\tau \sim \alpha$. The latter is where the walker undergoes a transition from a self-trapped state to solitonlike behavior. There is a discontinuity between both regimes represented by the shadowed area in the interval $\alpha \in [1, 2]$ where τ cannot be evaluated precisely.

FIG. 5. Time evolution of the single-pulse average position $\langle x(t) \rangle$ for some representative values of the nonlinearity level α. For strong nonlinearities, $\langle x(t) \rangle$ has a very slow initial increase during the self-trapping time. After that it evolves with a constant velocity. For weak nonlinearities, there is a crossover from $v = 1/2$ at short times to a larger velocity after the soliton formation. The inset shows this crossover around the soliton formation time for $\alpha = 0.01$.

the soliton formation time τ as the instant σ_{sp} reaches its maximum. This is a numerically convenient measure that enables us to deal with both regimes. For lower (higher) degrees of nonlinearity, τ seems to diminish (grow) upon increasing α.

To clearly distinguish between these two regimes, Fig. 4 shows how τ scales with α. For small values of α, we note that the timescale for soliton formation is characteristically longer, fulfilling $\tau \sim \alpha^{-2}$. At some point, this tendency breaks down. Roughly in the interval $\alpha \in [1, 2]$ the curve $\sigma_{\mathrm{sp}}(t)$ presents no peak to extract τ from. Interestingly, right after this interval the walker begins to display the self-trapping behavior before turning into solitonlike pulses [as clearly seen in Fig. 2(d)]. At this stage, τ grows linearly with α.

Having addressed the onset of soliton formation and its corresponding timescales, let us now evaluate how fast it moves. To do so, we track the single-pulse walker's average position $\langle x(t) \rangle = \sum_{x=0}^{\infty} x P_x(t)$ (first moment) and evaluate its velocity v in the long-time limit. Results for the time evolution of $\langle x(t) \rangle$ are shown in Fig. 5 for some representative values of the nonlinear coupling. The long-time asymptotic velocity as a function of α is reported in Fig. 6. The regimes of weak and strong nonlinearities are characterized by quite distinct dynamics. In the strongly nonlinear regime, $\langle x(t) \rangle$ presents a very slow initial increase in the time interval during which self-trapping is active. After this initial transient, a solitonic pulse evolves with a constant velocity. In the weakly nonlinear regime, the asymptotic velocity becomes larger than the corresponding one at $\alpha = 0$. First and foremost, it is convenient to have in mind that the velocity for the linear case ($\alpha = 0$) is $v = 1/2$ [3]. Now, for $\alpha \to 0$, it reaches $v = 1/\sqrt{2}$. This happens because the nonlinearity couples the frequency modes, thereby allowing for energy exchange between them such that it results in an energy drift [60,61] to
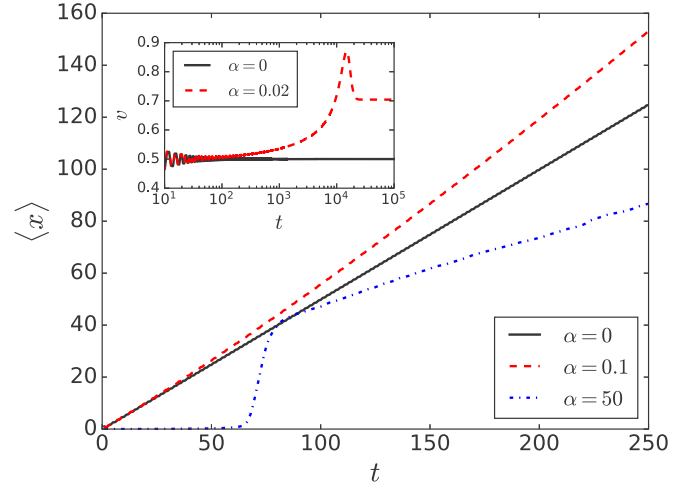
the bottom of the band where the group velocity is maximum, that is, $v_g = 1/\sqrt{2}$ [3]. For timescales much smaller than the typical soliton formation time τ, a weak nonlinear coupling does not significantly affect the dynamics and the spreading velocity $v \simeq 1/2$. However, for $t \gg \tau$ the velocity becomes larger, with an overshooting during the soliton formation. These features are illustrated in the inset of Fig. 5. It is important to have in mind that the soliton formation time diverges as $\tau \sim 1/\alpha^2$ when $\alpha \to 0$; therefore the order on which the limits of $t \to \infty$ and $\alpha \to 0$ are taken is relevant. Figure 6 was raised measuring the velocity after the soliton formation. Another interesting aspect we note is that the velocity takes
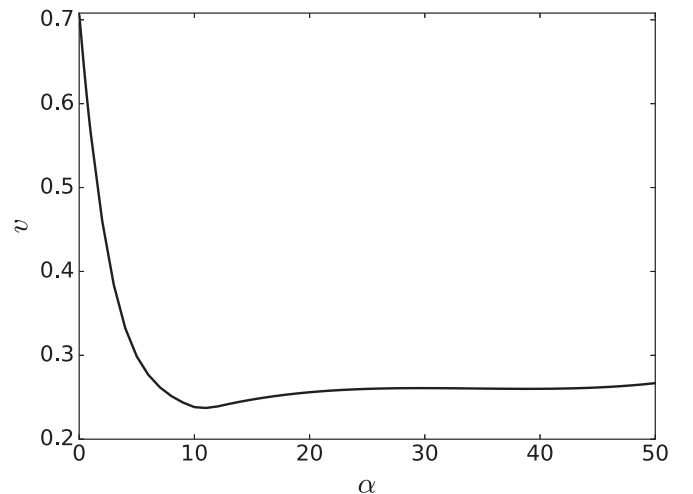

FIG. 6. Asymptotic velocity v of the single-pulse average position $\langle x(t) \rangle$ against nonlinearity level α, obtained via linear regression at long times ($t = 8600$ in some cases). The maximum velocity is found to be $v = 1/\sqrt{2}$ when $\alpha \to 0$.
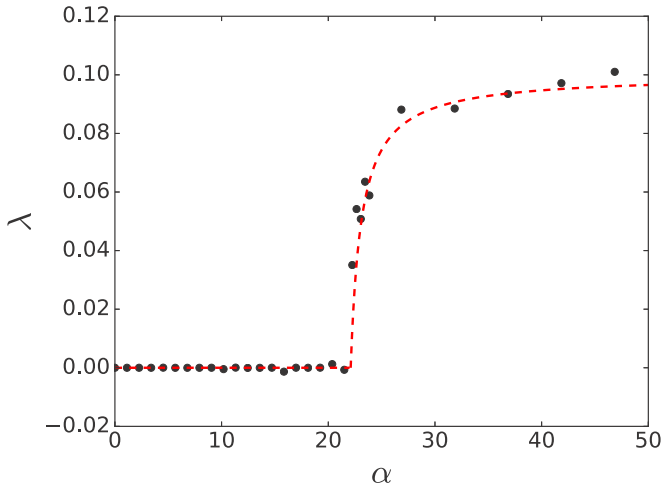
FIG. 7. Averaged Lyapunov exponent λ vs nonlinearity strength α. For each α we generated about 350 independent sets of $\{\delta_x\}$ (randomly distributed within $[-10^{-6}, 10^{-6}]$) to form $|\Psi_\delta(t_0)\rangle$ and thus evaluate the distance $d(t)$ (see text for details) starting at $t_0 = 500$. A linear fit is put in order for $\ln d(t)$ so as to find its slope λ, conveniently between steps $t = 600$ and $t = 800$. The system size is fixed to $N = 8000$ to avoid boundary effects, and the initial state $|\Psi(t = 0)\rangle = (|x_0, \uparrow\rangle + i|x_0, \downarrow\rangle)/\sqrt{2}$, with $x_0 = 0$. Chaotic features begin to set in above $\alpha_c \approx 23$. The line is for guiding the eye, and it follows that $0.1(\alpha - \alpha_c)/[1 + (\alpha - \alpha_c)]$ in the chaotic regime. Each point is the average over many neighboring outcomes.

$v = 1/2$ again between $\alpha = 1$ and 2, thus belonging to the interval corresponding to the regime's crossover (see Fig. 4). In addition, we see that higher velocities are assigned to the slow soliton formation regime characterized by $\tau \sim \alpha^{-2}$.

Another feature worth investigating is the behavior of $\langle x(t) \rangle$ and $\sigma_{\rm sp}(t)$ at early times (before soliton formation). At the low nonlinearity level, we may approximate the short-time probability distribution at the right side of the chain as having a uniform profile $P(x < x_m) = 1/x_m$ up to a wave-packet front position evolving ballistically as $x_m \propto t$. In this case $\langle x(t) \rangle \sim t$ and $\sigma_{\rm sp}(t) \sim t$, as one would also obtain for the linear DTQW. Such a short-time regime is interrupted by the soliton formation. Now for the regime where temporary self-trapping takes place ($\alpha > 2$), we may consider that $P(x < x_m) = a\delta(x) + b$ at short times, where $\delta(x)$ is the Dirac δ distribution accounting for the self-trapped component, b is a constant, and $a = 1 - bx_m$, resulting from the normalization of $P(x)$. That yields to the short-time dynamic behavior $\langle x(t) \rangle \sim t^2$ and $\sigma_{\rm sp}(t) \sim t^{3/2}$. This regime is short-lived, as the newly born solitonlike pulses travel off [see Fig. 2(d)] with uniform velocity.

IV. TRANSITION TO CHAOS

A trained eye may notice in the inset of Fig. 3 that after the solitonlike pulse has been fully established, as accounted for by $\sigma_{\rm sp}(t)$, it goes on following a periodic breathing pattern for $\alpha = 20$ while displaying an irregular profile for $\alpha = 30$. This scenario makes us wonder about the possibility of the quantum walker to display some sort of sensitivity to initial conditions for large enough α.
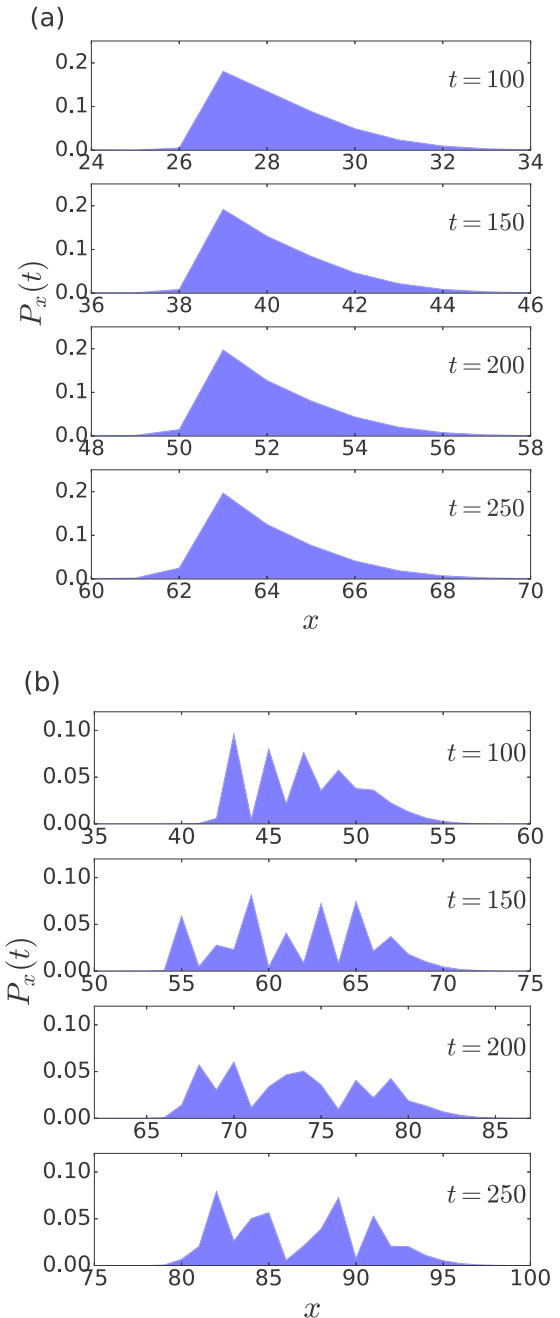

FIG. 8. Snapshots of the single pulse distribution for two representative values of the nonlinearity. (a) For $\alpha = 10$ the distribution keeps its form while propagating along the chain. (b) For $\alpha = 50$ the wave packet develops irregular fluctuations typical of the chaotic regime.

In order to properly set the boundary for such an unstable regime, we evaluate the Lyapunov exponent by adding a small perturbation to the wave function at a given instant so as to see if it diverges exponentially from the original form. In particular, at step t_0 we set another state of the form [cf. Eq. (1)],

$$|\Psi_\delta(t_0)\rangle = \sum_x \left(m_{x,\uparrow}^{(\delta)}(t_0)|x, \uparrow\rangle + m_{x,\downarrow}^{(\delta)}(t_0)|x, \downarrow\rangle \right), \quad (6)$$
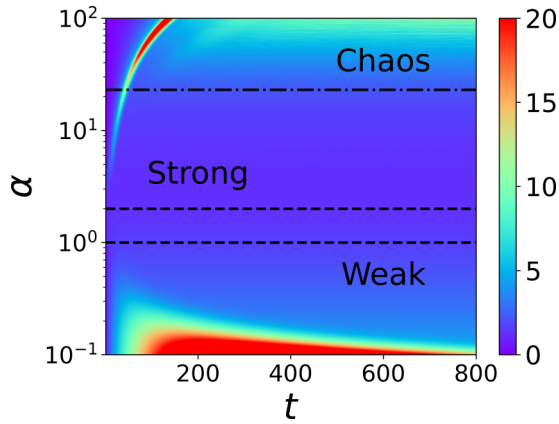
FIG. 9. Density plot of the single pulse dispersion as a function of time t and nonlinearity α. Peaks in dispersion separate the initial transient regimes from the solitonic regime. The initial transient features spread (self-trapped) distributions for weak (strong) nonlinearities. Dispersion has no peak at intermediate nonlinear strengths. The chaotic regime is characterized by irregular fluctuations of the wave-packet dispersion.

where $m_{x,(\uparrow,\downarrow)}^{(\delta)} = m_{x,(\uparrow,\downarrow)}(1 + \delta_x)$, with $\delta_x \in \mathbb{R}$ being a random number falling in the box distribution $[-10^{-6}, 10^{-6}]$. We normalize it afterwards, $|\Psi_\delta\rangle \rightarrow |\Psi_\delta\rangle/\sqrt{\langle\Psi_\delta|\Psi_\delta\rangle}$, and carry on with $|\Psi_\delta(t, t_0)\rangle = U_{nl}^{t-t_0}|\Psi_\delta(t_0)\rangle$ and $|\Psi(t, t_0)\rangle = U_{nl}^{t-t_0}|\Psi(t_0)\rangle$ separately, evaluating the distance between both states via $d(t) \equiv |\langle\Psi_d|\Psi_d\rangle|^2$ at each step, for the non-normalized state $|\Psi_d(t, t_0)\rangle = |\Psi_\delta(t, t_0)\rangle - |\Psi(t, t_0)\rangle$. To finally find the Lyapunov exponent λ we assume $d(t) = d(t_0)e^{\lambda t}$. Figure 7 shows λ against the degree of nonlinearity α averaged over many independent samples of $\{\delta_x\}$ for each α. There is indeed a chaotic regime starting from $\alpha_c \approx 23$ above which λ values become positive.

To illustrate the distinct wave-packet dynamics in the regular and chaotic regimes, we plot some snapshots of the single pulse distribution for two distinct values of the nonlinear strength below and above the transition to chaos (see Fig. 8). In both cases, the wave-packet width is time independent, as expected for solitonic pulses. However, for $\alpha < \alpha_c$ the pulse keeps its form while traveling along the chain while it develops irregular fluctuations in the chaotic regime.

We summarize the distinct dynamical regimes reported above in Fig. 9, where we show a density plot of the single pulse dispersion as a function of time t and nonlinearity α. The regime of weak nonlinearity is characterized by an initial spreading of the wave-packet distribution followed by a transient soliton formation period after which the pulse propagates at a constant velocity. The dispersion develops a wide peak during the soliton formation. In the strongly

nonlinear regime, the distribution presents a transient self-trapping period, after which a solitonic pulse starts to move. The dispersion presents a sharp peak during the transition from self-trapping to solitonic behavior. There is a regime of intermediate nonlinear strengths on which the dispersion has no peak. For very strong nonlinearities, the chaotic regime is signalled by irregular fluctuations of the pulse dispersion.

Last, me mention that the DTQW dynamics remains (quasi)ballistic despite the presence of nonlinearity, thereby maintaining its quantum hallmark. Using a different nonlinear and unitary DTQW model accounting for a specific configuration of the optical Galton board, the authors of Ref. [26] also found no deterioration of the quantum walk property $\sigma \propto t$ with the formation of solitonlike pulses.

V. CONCLUDING REMARKS

The Hadamard DTQW model with modified shift operator to encompass a third-order nonlinear contribution which underlies many physical phenomena was shown to display a wide range of dynamical regimes. Solitonlike pulses were found for any degree of nonlinearity α and preceded by temporary self-trapping for $\alpha > 2$, during which $\langle x(t)\rangle \sim t^2$ and the soliton formation time $\tau \sim \alpha$. The regime of small α is characterized by $\tau \sim \alpha^{-2}$ and for featuring higher velocities of the single-pulse first moment $\langle x(t)\rangle$ in the asymptotic long-time limit, reaching $v = 1/\sqrt{2}$ for $\alpha \rightarrow 0$.

Such speedup may find applications in quantum search protocols. As a matter of fact, it has been investigated in the realm of the Gross-Pitaevskii equation [62,63]. The very presence of cubic nonlinearity of the form $|\psi|^2\psi$ is such that it outperforms the Schrödinger equation in solving the unstructured search problem.

Another remarkable feature emerging from the third-order nonlinearity is the sharp onset of a chaotic regime taking place after stabilization of the solitonlike pulse. We evaluated the Lyapunov coefficients for a range of α values and got $\alpha \approx 23$ as the nonlinearity degree that marks the transition from regular to chaotic dynamics. We mention that chaotic behavior was also identified in a different model in Ref. [26].

We hope that the above findings fuel further research in nonlinear DTQWs as potential platforms for observing the clear signatures of quantum chaos and other nonlinear phenomena, especially in view of the recent progress of experimental implementations of nonunitary quantum walks via photonic devices [5,7,8].

[1] Y. Aharonov, L. Davidovich, and N. Zagury, Phys. Rev. A **48**, 1687 (1993).

[2] J. Kempe, Contemp. Phys. **44**, 307 (2003).

[3] S. E. Venegas-Andraca, Quantum Inf. Process. **11**, 1015 (2012).

[4] C. M. Chandrashekar and R. Laflamme, Phys. Rev. A **78**, 022314 (2008).

[5] K. Wang, X. Qiu, L. Xiao, X. Zhan, Z. Bian, W. Yi, and P. Xue, Phys. Rev. Lett. **122**, 020501 (2019).

[6] E. Flurin, V. V. Ramasesh, S. Hacohen-Gourgy, L. S. Martin, N. Y. Yao, and I. Siddiqi, Phys. Rev. X **7**, 031023 (2017).

[7] L. Xiao, X. Zhan, Z. H. Bian, K. K. Wang, X. Zhang, X. P. Wang, J. Li, K. Mochizuki, D. Kim, N. Kawakami, W. Yi, H. Obuse, B. C. Sanders, and P. Xue, Nat. Phys. **13**, 1117 (2017).

[8] X. Zhan, L. Xiao, Z. Bian, K. Wang, X. Qiu, B. C. Sanders, W. Yi, and P. Xue, Phys. Rev. Lett. **119**, 130501 (2017).

[9] G. Di Molfetta, M. Brachet, and F. Debbasch, Phys. Rev. A **88**, 042301 (2013).

[10] N. Shenvi, J. Kempe, and K. Birgitta Whaley, Phys. Rev. A **67**, 052307 (2003).

[11] A. Ambainis, Int. J. Quantum Inf. **1**, 507 (2003).

[12] A. M. Childs, Phys. Rev. Lett. **102**, 180501 (2009).

[13] N. B. Lovett, S. Cooper, M. Everitt, M. Trevers, and V. Kendon, Phys. Rev. A **81**, 042330 (2010).

[14] D. Meyer, J. Stat. Phys. **85**, 551 (1996).

[15] F. W. Strauch, Phys. Rev. A **73**, 054302 (2006).

[16] C. M. Chandrashekar, S. Banerjee, and R. Srikanth, Phys. Rev. A **81**, 062340 (2010).

[17] C. A. Ryan, M. Laforest, J. C. Boileau, and R. Laflamme, Phys. Rev. A **72**, 062317 (2005).

[18] H. Schmitz, R. Matjeschk, C. Schneider, J. Glueckert, M. Enderlein, T. Huber, and T. Schaetz, Phys. Rev. Lett. **103**, 090504 (2009).

[19] S. Dadras, A. Gresch, C. Groiseau, S. Wimberger, and G. S. Summy, Phys. Rev. Lett. **121**, 070402 (2018).

[20] T. Giordani, E. Polino, S. Emiliani, A. Suprano, L. Innocenti, H. Majury, L. Marrucci, M. Paternostro, A. Ferraro, N. Spagnolo, and F. Sciarrino, Phys. Rev. Lett. **122**, 020503 (2019).

[21] G. Grossing and A. Zeilinger, Complex Systems **2**, 197 (1988).

[22] S. Fussy, G. Grossing, H. Schwabl, and A. Scrinzi, Phys. Rev. A **48**, 3470 (1993).

[23] D. Meyer, Phys. Rev. E **55**, 5261 (1997).

[24] P. C. S. Costa, R. Portugal, and F. de Melo, Quantum Inf. Proc. **17**, 226 (2018).

[25] I. Vakulchyk, M. V. Fistul, and S. Flach, Phys. Rev. Lett. **122**, 040501 (2019).

[26] C. Navarrete-Benlloch, A. Pérez, and E. Roldán, Phys. Rev. A **75**, 062333 (2007).

[27] Y. Shikano, T. Wada, and J. Horikawa, Sci. Rep. **4**, 4427 (2014).

[28] C. W. Lee, P. Kurzyński, and H. Nha, Phys. Rev. A **92**, 052336 (2015).

[29] G. Di Molfetta, F. Debbasch, and M. Brachet, Phys. Rev. E **92**, 042923 (2015).

[30] Y. Gerasimenko, B. Tarasinski, and C. W. J. Beenakker, Phys. Rev. A **93**, 022329 (2016).

[31] A. D. Verga, Eur. Phys. J. B **90**, 41 (2017).

[32] R. Adami, R. Fukuizumi, and E. Segawa, Quantum Inf. Proc. **18**, 119 (2019).

[33] A. R. C. Buarque and W. S. Dias, Phys. Rev. A **101**, 023802 (2020).

[34] M. Maeda, H. Sasaki, E. Segawa, A. Suzuki, and K. Suzuki, Discrete Contin. Dyn. Syst. **38**, 3687 (2018).

[35] M. Maeda, H. Sasaki, E. Segawa, A. Suzuki, and K. Suzuki, Quantum Inf. Proc. **17**, 215 (2018).

[36] D. K. Campbell, A. R. Bishop, and K. Fesser, Phys. Rev. B **26**, 6862 (1982).

[37] V. M. Kenkre and D. K. Campbell, Phys. Rev. B **34**, 4959 (1986).

[38] J. Meier, G. I. Stegeman, Y. Silberberg, R. Morandotti, and J. S. Aitchison, Phys. Rev. Lett. **93**, 093903 (2004).

[39] Z. G. Chen, M. Segev, and D. N. Christodoulides, Rep. Prog. Phys. **75**, 086401 (2012).

[40] A. Trombettoni and A. Smerzi, Phys. Rev. Lett. **86**, 2353 (2001).

[41] J.-K. Xue and A.-X. Zhang, Phys. Rev. Lett. **101**, 180401 (2008).

[42] G. K. Brennen and J. E. Williams, Phys. Rev. A **68**, 042311 (2003).

[43] V. Kendon, Math. Struct. Comput. Sci. **17**, 1169 (2007).

[44] X. Zhan, J. Phys. Commun. **3**, 085013 (2019).

[45] K. Mochizuki, D. Kim, and H. Obuse, Phys. Rev. A **93**, 062116 (2016).

[46] T. Nitsche, S. Barkhofen, R. Kruse, L. Sansoni, M. Štefaňák, A. Gábris, V. Potoček, T. Kiss, I. Jex, and C. Silberhorn, Sci. Adv. **4**, eaar6444 (2018).

[47] A. Regensburger, C. Bersch, M.-A. Miri, G. Onishchukov, D. N. Christodoulides, and U. Peschel, Nature (London) **488**, 167 (2012).

[48] A. Regensburger, M. A. Miri, C. Bersch, J. Näger, G. Onishchukov, D. N. Christodoulides, and U. Peschel, Phys. Rev. Lett. **110**, 223902 (2013).

[49] M. Wimmer, A. Regensburger, M.-A. Miri, C. Bersch, D. N. Christodoulides, and U. Peschel, Nat. Commun. **6**, 7782 (2015).

[50] A. L. M. Muniz, M. Wimmer, A. Bisianov, U. Peschel, R. Morandotti, P. S. Jung, and D. N. Christodoulides, Phys. Rev. Lett. **123**, 253903 (2019).

[51] F. Flamini, N. Spagnolo, and F. Sciarrino, Rep. Prog. Phys. **82**, 016001 (2019).

[52] A. Schreiber, K. N. Cassemiro, V. Potoček, A. Gábris, P. J. Mosley, E. Andersson, I. Jex, and C. Silberhorn, Phys. Rev. Lett. **104**, 050502 (2010).

[53] A. Regensburger, C. Bersch, B. Hinrichs, G. Onishchukov, A. Schreiber, C. Silberhorn, and U. Peschel, Phys. Rev. Lett. **107**, 233902 (2011).

[54] M.-A. Miri, A. Regensburger, U. Peschel, and D. N. Christodoulides, Phys. Rev. A **86**, 023807 (2012).

[55] M. Wimmer, M.-A. Miri, D. Christodoulides, and U. Peschel, Sci. Rep. **5**, 17760 (2015).

[56] T. Nitsche, F. Elster, J. Novotný, A. Gábris, I. Jex, S. Barkhofen, and C. Silberhorn, New J. Phys. **18**, 063017 (2015).

[57] J. Boutari, A. Feizpour, S. Barz, C. Di Franco, M. S. Kim, W. S. Kolthammer, and I. A. Walmsley, J. Opt. **18**, 094007 (2016).

[58] A. Bisianov, M. Wimmer, U. Peschel, and O. A. Egorov, Phys. Rev. A **100**, 063830 (2019).

[59] A. V. Pankov, I. D. Vatnik, D. V. Churkin, and S. A. Derevyanko, Opt. Express **27**, 4424 (2019).

[60] M. Mulansky, K. Ahnert, A. Pikovsky, and D. L. Shepelyansky, Phys. Rev. E **80**, 056212 (2009).

[61] M. Mulansky and A. Pikovsky, Eur. Phys. J. B **85**, 105 (2012).

[62] D. A. Meyer and T. G. Wong, New J. Phys. **15**, 063014 (2013).

[63] D. A. Meyer and T. G. Wong, Phys. Rev. A **89**, 012312 (2014).